ACS NANO

www.acsnano.org

ARTICLE

High-Resolution Cryogenic Spectroscopy of Single Molecules in Nanoprinted Crystals

Mohammad Musavinezhad, Jan Renger, Johannes Zirkelbach, Tobias Utikal, Claudio U. Hail, Thomas Basché, Dimos Poulikakos, Stephan Götzinger, and Vahid Sandoghdar*

Cite This: https://doi.org/10.1021/acsnano.4c02003

Read Online

ACCESS | Metrics & More | Article Recommendations | Supporting Information

ABSTRACT: We perform laser spectroscopy at liquid helium temperatures (T = 2 K) to investigate single dibenzoterrylene (DBT) molecules doped in anthracene crystals of nanoscopic height fabricated by electrohydrodynamic dripping. Using high-resolution fluorescence excitation spectroscopy, we show that zero-phonon lines of single molecules in printed nanocrystals are nearly as narrow as the Fourier-limited transitions observed for the same guest–host system in the bulk. Moreover, the spectral instabilities are comparable to or less than one line width. By recording super-resolution images of DBT molecules and varying the polarization of the excitation beam, we determine the dimensions of the printed crystals and the orientation of the crystals' axes. Electrohydrodynamic printing of organic nano- and microcrystals is of interest for a series of applications, where controlled positioning of quantum emitters with narrow optical transitions is desirable.

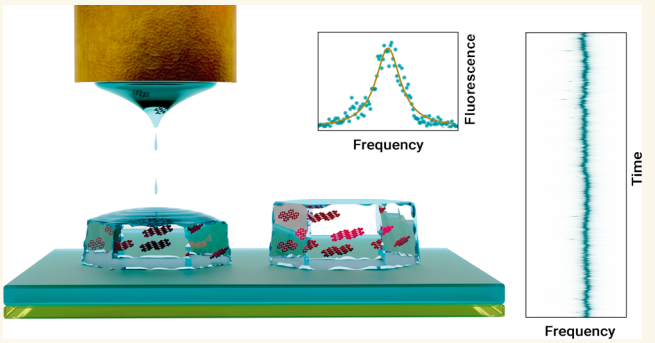

KEYWORDS: *nanoprinting, nanocrystal, quantum emitter, single molecule, single-photon source, spectroscopy*

Molecules embedded in organic crystals hold great promise to act as solid-state emitters for applications in integrated quantum photonic circuits.[1,2] In particular, individual dye molecules can possess lifetime-limited narrow electronic transitions in the order of 10 MHz at liquid helium temperatures,[2−4] comparable to that of unperturbed alkali atoms. The fact that molecules can be synthesized with atomic precision and have a very small footprint of about 1 nm, makes them ideally suited for a number of interesting applications. Indeed, single dye molecules are selectively addressable at cryogenic temperatures and have been utilized for the realization of a bright single-photon source,[5] achieving strong coupling and single-photon nonlinearities in a microcavity.[6] Some of the exciting future applications such as quantum networks require the collective coherent coupling of several quantum nodes to a common photonic mode.[7,8] However, efficient coupling of a large number of emitters will require a high degree of control over both their resonance frequencies and positions.

In an earlier work, we showed that *p*-terphenyl nanocrystals (NCs) doped with a very small number of terrylene molecules could be printed by electrohydrodynamic dripping (EHD) and positioned with respect to photonic structures with sub-wavelength accuracy.[9] Moreover, we showed that terrylene molecules in this system were well protected and remained photostable at room temperature. However, the spectral behavior of the guest molecules remained unexplored. In particular, the key question of whether the electronic transitions could reach their Fourier limit in such nanocrystals has not been addressed. Indeed, quantum emitters are known to experience dephasing and line broadening close to interfaces and in nanoscopic environments.[10−12] In this article, we extend our material system to that of dibenzoterrylene (DBT) in anthracene (Ac) and demonstrate that the zero-phonon lines (00ZPLs) connecting the ground state $|g, \nu = 0\rangle$ and the lowest vibrational level of the excited state $|e, \nu = 0\rangle$ in DBT molecules become nearly as narrow as the expected Fourier limit in bulk samples. This feature combined with subwavelength accuracy in positioning can be utilized for large-scale coupling of molecules to photonic devices.

Received: February 9, 2024
Revised: May 30, 2024
Accepted: July 2, 2024

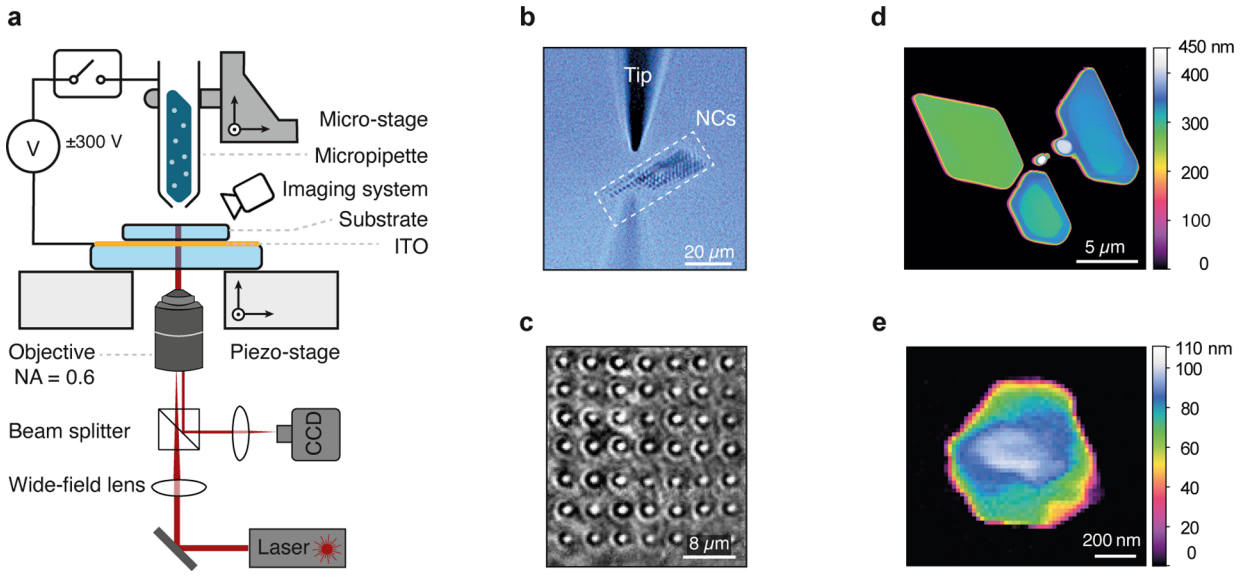

Figure 1. Electrohydrodynamic nanodripping for fabrication of organic crystals. (a) Sketch of the setup utilized for printing organic crystals. The setup integrates a low-resolution side channel and a high-resolution iSCAT channel for real-time imaging of printed structures during fabrication. (b) An example of the side-view for facilitating the coarse alignment of the micropipette (tip) above the sample substrate. The dashed rectangle marks the region of the printed array of nanocrystals (NCs). (c) An example of the iSCAT image of a printed array of Ac NCs. (d) Atomic force microscope image of printed AC microcrystals. (e) Atomic force microscope image of a printed AC NC. Color bars indicate the measured height.

RESULTS AND DISCUSSION

Electrohydrodynamic nanodripping is a versatile printing technique that utilizes an applied electric field at the tip of a micropipette to deposit individual subfemtoliter droplets of an "ink" onto a surface. Upon evaporation of the solvent, particles or molecules coagulate to form nanostructures. This method allows for precise subwavelength placement of the nano-object and is applicable to a wide range of materials, including gold nanoparticles,[13,14] quantum dots,[15,16] and organic molecules.[9] In this work, we explore the spectral behavior of DBT molecules in printed Ac crystals at cryogenic temperatures. DBT is a member of the polycyclic aromatic hydrocarbons (PAH) group and possesses exceptional spectral stability, strong 00ZPLs, high quantum efficiency,[17] and negligible dephasing when incorporated in suitable matrices at T = 2 K.[2,18]

Principles of nanoprinting have been previously discussed, e.g., in ref 13. Figure 1a displays a schematic of the fabrication setup. In brief, the sample is placed on a transparent fused silica substrate with a 100 nm indium tin oxide (ITO) coating that serves as a ground electrode. A gold-coated glass microcapillary nozzle (tip diameter: 1.5 ± 0.5 μm) is filled with the printing ink. In this work, we used a 10:1 mixture of 1-octanol saturated with Ac, and 2 μM DBT in trichlorobenzene (TCB) as the ink (see Experimental Section). The tip is then placed approximately 5 μm above the sample surface, while monitored by a side-view imaging system (see Figure 1b). A DC voltage is applied across the nozzle and the ground electrode to trigger the ejection of ink droplets. Periodic ejection of nanodroplets can be achieved at rates exceeding 100 Hz, depending on the applied DC voltage and properties of the ink.[13] Precise placement of the droplets is facilitated by piezoelectric positioners to adjust the sample relative to the nozzle. The nanocrystal growth is continuously monitored in real-time with an iSCAT microscope,[19] as demonstrated in Figure 1c.

As the solvent gradually evaporates, the ink droplet reaches supersaturation and the solute molecules precipitate to form crystals. Similar to other solution-based techniques, the quality of the printed crystals is significantly influenced by various factors including the choice of the solvent,[20] evaporation rate,[9] concentration, and the organic compound to be printed. Additionally, maintaining a limited dilution level of the ink is crucial to prevent clogging of the nozzle. Increasing the concentration of Ac above ~7 mg/mL may disrupt the ink flow and prevent the printing process. Moreover, a solvent with low surface tension is needed to enable ejection at voltages below the ionization threshold of the ambient atmosphere. In addition, a slower crystal growth is advantageous for achieving a high-quality molecular arrangement. The latter can be accomplished by using solvents with low evaporation rates at ambient conditions. It is also possible to increase the duration of crystal growth by maintaining the concentration of host molecules close to the saturation level. By doing so, the ink droplet reaches supersaturation as soon as evaporation starts and the growth time is merely limited by the full evaporation of the solvent. The solubility of 1-octanol for Ac reaches saturation at around 2.3 mg/mL, which falls well within the optimal concentration range for nanoprinting. Other favorable properties of this substance include low surface tension and slow evaporation rate.

The size of the printed crystal can be adjusted by controlling the voltage amplitude and the dripping time. If, as for 1-octanol, the evaporation of the solvent is slow, consecutive nanodroplets can accumulate before the crystal is fully formed. Consequently, crystalline structures from several micrometers down to hundreds of nanometers can be produced. Figure 1d-e presents examples of printed microcrystals and NCs, measured via atomic force microscopy. In a first demonstration, we present the cryogenic characterization of a highly doped DBT:Ac microcrystal that is about 5 μm wide and less than 500 nm in height.

https://doi.org/10.1021/acsnano.4c02003
ACS Nano XXXX, XXX, XXX−XXX

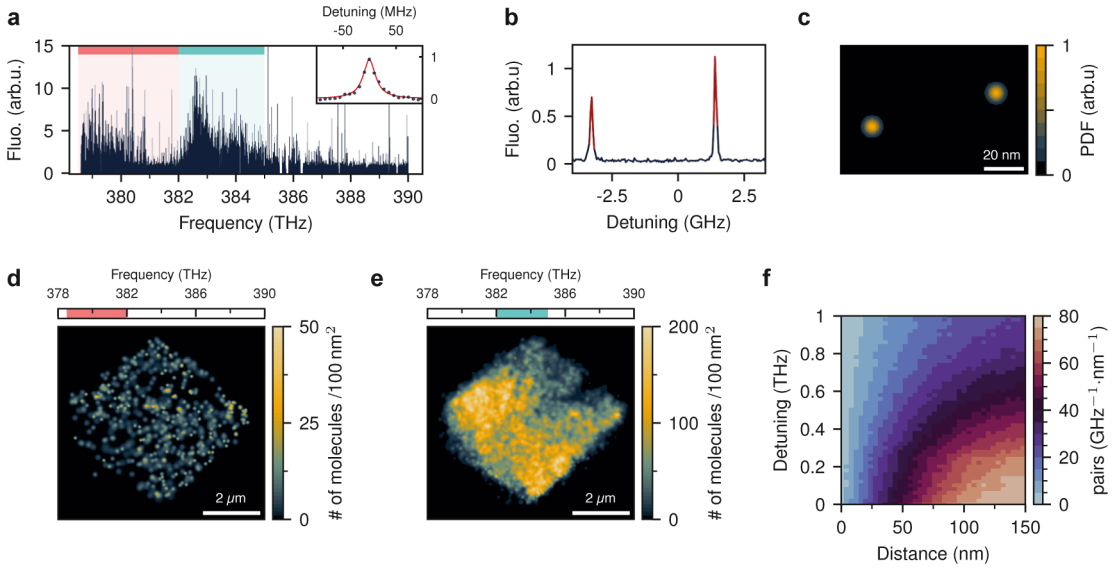

Figure 2. Spatial and spectral distribution of DBT molecules in printed organic crystals. (a) Fluorescence excitation spectrum from 1 μm^2 of a printed DBT:Ac microcrystal recorded at 2 K. The inset shows an example of a high-resolution spectrum of a single-molecule 00ZPL. The gaps in the scanning range are due to interruptions in the laser cavity lock. The two main insertion sites of DBT in Ac are marked with red and turquoise regions. (b) Spectra of two molecules located within a diffraction-limited spot. Red curves show the data points used to localize individual molecules. (c) Probability density function (PDF) of lateral positions for the two DBT molecules in (b). The location of each emitter is represented by a Gaussian spot. (d) Super-resolution image of 589 molecules between 378.5 THz and 382 THz, i.e., the red region in (a). The embedded emitters mark the crystal's shape and boundaries. (e) Super-resolution image of 11197 molecules between 382 THz and 385 THz, i.e., the turquoise region in (a). (f) Distribution of frequency detuning and distance between molecular pairs for emitters with less than 150 nm lateral separation.

To conduct spectroscopic measurements on the embedded DBT molecules, the sample was cooled to 2 K in a helium bath cryostat. The crystal was illuminated in the wide-field mode by a beam from a frequency-tunable narrow-band (<1 MHz) Ti:sapphire laser. The back-reflected laser beam was blocked by a tunable long-pass filter, and the red-shifted fluorescence signal was measured with an avalanche photodiode detector (APD) or an EMCCD camera as the laser frequency was scanned. Device synchronization and measurement automation were done using a custom software based on pyLabLib.[21] A more detailed description of the optical setup is presented elsewhere.[17]

Figure 2a presents the fluorescence excitation spectra of molecules within a region of 1 μm^2 from a microcrystal recorded by the camera. Due to slight variations in the local environment, the transition frequencies of individual molecules vary within the inhomogeneous broadening (IB). For DBT:Ac, IB ranges from approximately 100 GHz up to a few THz, depending on the crystalline quality and the insertion site.[18,22] We attribute the two spectral subpopulations in Figure 2a to the two main insertion sites of DBT in Ac. A similar feature was previously observed in bulk Ac with sites at about 381.9 and 377.4 THz.[18] The slight blue shift of the resonance frequencies in printed microcrystals is consistent with our previous observations of a similar effect in submicron thin crystals.[23]

If the doping level is not too high, the 00ZPLs of individual molecules do not overlap so that single molecules can be identified and addressed in frequency space.[24] The symbols in the inset of Figure 2a show an example of a high-resolution scan through the 00ZPL of a single molecule, fitted with a Lorentzian function (red curve) of full width at half-maximum (fwhm), corresponding to $\gamma = (28 \pm 1)$ MHz.

The large DBT doping level of the crystal allows us to establish a super-resolution image of the Ac crystal.[25] As demonstrated in Figure 2b, we can identify two individual molecules through their nonoverlapping 00ZPLs. The fluorescence point-spread function (PSF) of a molecule in a batch of frames is fitted by a two-dimensional (2D) Gaussian function, and its center is localized, determining the probability density function (PDF) of a molecule's positions in the sample plane. The outcome yields a Gaussian spot, whereby its standard deviation (σ) is obtained from the localization precision. Figure 2c illustrates the super-resolution image of the two molecules (same as in Figure 2b) separated by (69 ± 4) nm.

Figure 2d (2e) displays the super-resolution image of DBT molecules in the "red" ("blue") site, corresponding to transition frequencies below (above) 382 THz. We find that the molecules in the red site are nearly uniformly distributed. The great majority of the molecules (about 95%), however, reside within the blue site and experience a less uniform distribution. These sites correspond to two different configurations for substitution of DBT in the Ac lattice, and the population difference is attributed to their distinct thermodynamic potentials.[26]

In Figure 2f, we present a histogram of molecular pairs with less than 150 nm lateral separation. We find that the crystal contains more than 1000 pairs of molecules that are separated by less than 10 nm in the sample plane and at the same time, exhibit a frequency difference of less than 10 GHz. These conditions can be conducive to dipole−dipole coupling among two or more molecules.[27−29] However, we did not investigate this phenomenon any further in this work. We note that the observed trend between frequency and distance in Figure 2f is an artifact caused by the geometric growth factor $\propto 2\pi r$, where r is the separation.

https://doi.org/10.1021/acsnano.4c02003
ACS Nano XXXX, XXX, XXX−XXX

We now turn our attention to printed NCs. Due to their high surface-to-volume ratio, NCs typically sublimate within a few minutes following deposition under ambient conditions. To circumvent this, we applied a layer of poly(vinyl alcohol) (PVA) to the printed samples, facilitating their transfer to the cryostat under vacuum. Figure 3a presents an example of the

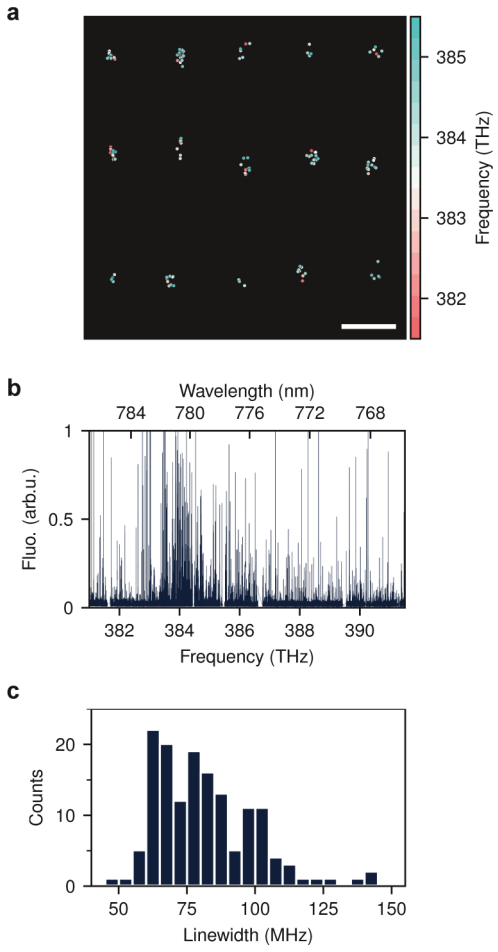

Figure 3. Spectral properties of printed DBT:Ac nanocrystals. (a) Distribution of emitters in an array of printed nanocrystals. Each DBT molecule is shown as a point. Color code shows the resonance frequency. The scale bar shows 4 μm. (b) Fluorescence of DBT molecules in 100 NCs as a function of excitation frequency. (c) Line width distribution of 150 DBT molecules embedded in the printed Ac NCs.

2D distribution of molecules in an array of DBT:Ac nanocrystals, whereby individual DBT molecules are illustrated as small circles color-coded according to their transition frequencies.

Figure 3b displays the excitation spectra of 100 NCs. For a more quantitative analysis of the homogeneous line width, we performed laser frequency scans at a slower rate (700 MHz/sec) over a frequency range of 383 to 387 THz for at least 10 repetitions. To minimize the effect of power broadening, the illumination intensity was set to 0.7 W·cm^{-2}, keeping the molecular excitation level well below saturation. Individual peaks in the excitation spectrum were then fitted with a Lorentzian function to extract their fwhm. Figure 3c presents a histogram of the measured line widths (γ) for 150 molecules recorded in at least 5 independent measurements (see Supporting Information). We measure molecular line widths as low as about 47 MHz, which is slightly larger than the lifetime-limited line width of DBT in bulk Ac (~30 MHz).[18]

A competitive feature of organic molecules as quantum emitters is their high emission rates and efficient interaction with light, which can also lead to a strong nonlinear response.[6,30] Therefore, we investigated γ and the detected fluorescence rate at resonance (F_{det}) as a function of excitation power. Figure 4a shows several excitation spectra of a molecule at different pump powers. As illustrated in Figure 4b, both line width broadening and count rates align with the expected saturation law given by

$$F_{det}(P) = F_{det}(\infty)\frac{P}{P + P_{sat}} \quad (1)$$

$$\gamma(P) = \gamma_0\sqrt{\frac{P + P_{sat}}{P_{sat}}} \quad (2)$$

where γ_0 is the intrinsic line width at weak excitation, and P_{sat} denotes the excitation power at saturation, i.e., $F_{det}(P_{sat}) = F_{det}(\infty)/2$. The low value of P_{sat} = 3.6 nW and the large number of detected photons $F_{det}(\infty)$ = 257 kcps (kilo counts per second) at full saturation are consistent with similar measurements conducted on DBT in bulk samples. This is also a strong indication that the quantum efficiency of the embedded molecules is similar to bulk.[17]

The high sensitivity of molecular transitions to minute changes in their nanoscopic environment allows for sensing a wide range of parameters such as strain,[31] electric fields and charges,[32] and temperature.[33] However, accurate measurements of spectral changes require stable resonances. To investigate this in printed NCs, we repeatedly scanned the laser frequency over several individual 00ZPLs. Figure 4c demonstrates the spectral stability of a single molecule during the course of 1 h, where the confocal excitation beam (0.6 nW) was kept fixed, and the red-shifted fluorescence was detected using an APD. The histogram of Figure 4d shows the distribution of measured central frequencies with a standard deviation of σ_f = 26 MHz, indicating that the resonance instability is comparable to one line width, which in this case amounted to γ = 47 MHz.

We performed similar analyses for 15 molecules to gain more statistical information on the spectral stability of DBT in printed Ac NCs. An example of the excitation spectra for 4 molecules located in different NCs is presented in Figure 4e. Only one of the emitters showed spectral jumps and all of them are photostable as long as the sample temperature remains below 30 K. Figure 4f summarizes the observed resonance instabilities σ_f with a median value at approximately 48 MHz. Normalizing the spectral diffusion range of each molecule ($2\sigma_f$) by its line width yields a median value of $2\sigma_f/\gamma$ = 1.08, underlining the molecules' good spectral stability.

Low spectral diffusion and narrow resonances are good indicators of high crystalline quality of the host matrix. Moreover, the orientation of the DBT molecules can report on the crystallinity of the surrounding Ac matrix. In highly crystalline Ac samples, DBT molecules are predominantly incorporated along the *b*-axis.[26] Thus, it is possible to deduce the orientation of the Ac crystal axis in the laboratory frame by determining the orientation of the transition dipole ϕ in the embedded DBT molecules. To achieve this, we rotated the polarization of the excitation beam θ_{exc} and recorded the corresponding fluorescence count rate. Figure 5a depicts the

https://doi.org/10.1021/acsnano.4c02003
ACS Nano XXXX, XXX, XXX−XXX

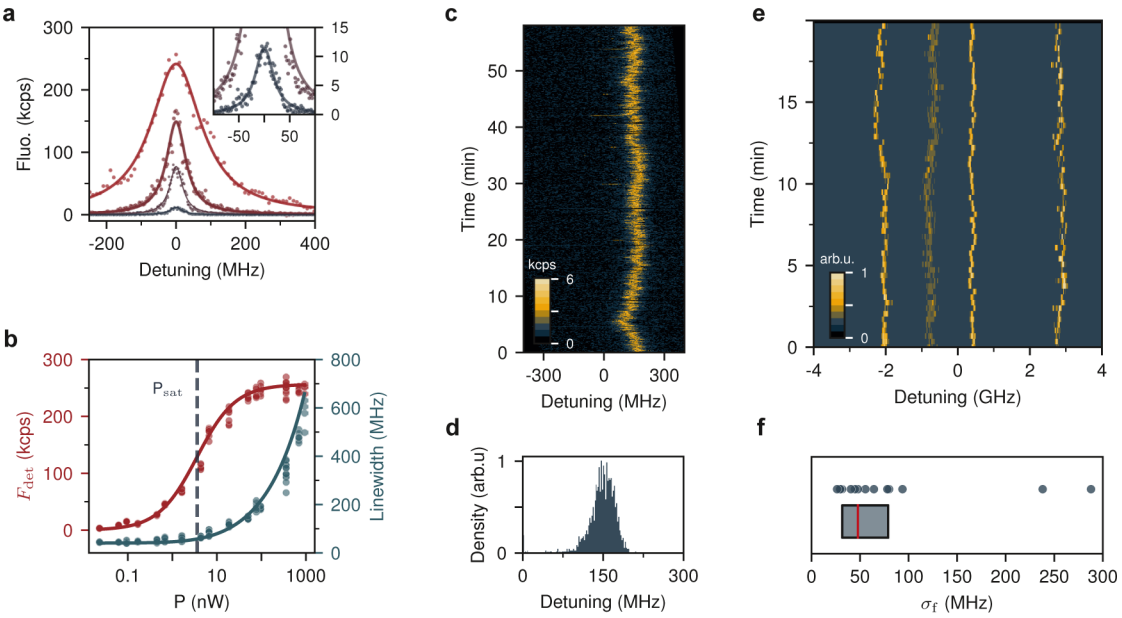

Figure 4. Saturation behavior and spectral stability of DBT molecules in printed nanocrystals. (a) Detected fluorescence as a function of laser detuning from the resonance of a single molecule, recorded at excitation powers P = (0.17, 1.6, 6.6, 95) nW. Solid lines show Lorentzian fits. (b) Saturation of the fluorescence count rate and power broadening at high pump powers. Lines show theoretical fits with saturation power P_{sat} = 3.6 nW and maximum fluorescence rate of F_∞ = 257 kcps and an intrinsic line width of γ_0 = 41 MHz. (c) Spectrum of a single molecule recorded at low excitation powers over 1 h. (d) Histogram of the Lorentzian fit centers for 1600 scans in (c). The standard deviation of the measured values is σ_f = 26 MHz. (e) Spectra of 4 molecules recorded over 20 min. (f) Resonance frequency fluctuations σ_f due to spectral diffusion for 15 DBT molecules in different NCs. The red line indicates the median at 48 MHz. The box represents the range between 25 and 75 percentile of the population.

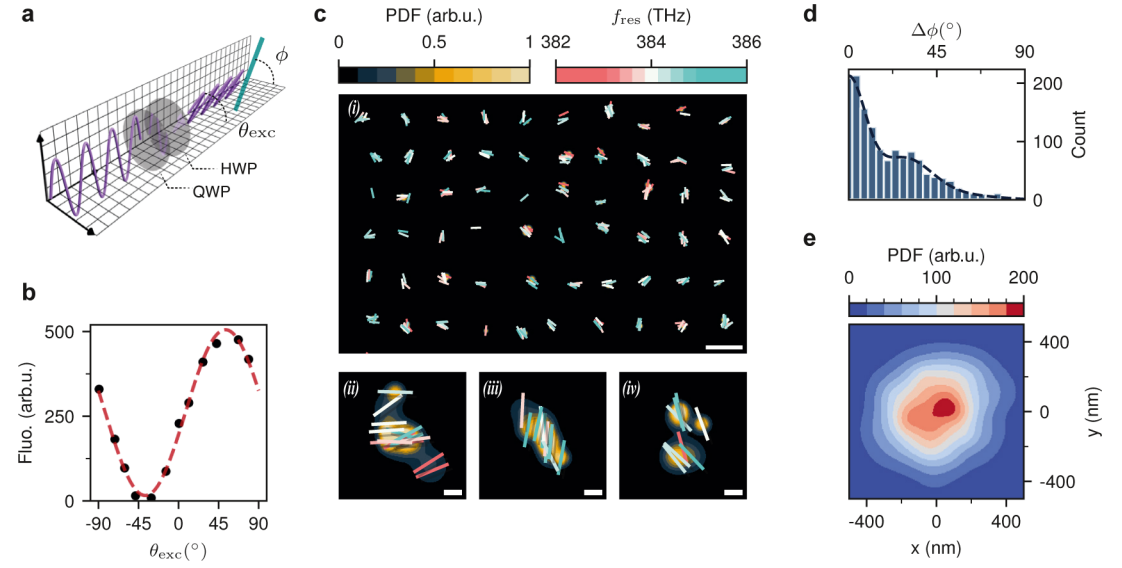

Figure 5. (a) Arrangement for determining the transition dipole moment orientation. A quarter-wave plate (QWP) and a half-wave plate (HWP) are used to adjust the excitation polarization θ_{exc}. ϕ indicates the angle of the transition dipole. (b) Fluorescence signal of a single molecule for different θ_{exc}. The dashed line is a fit to a $\cos^2$ function. (c) *i*: Simultaneous mapping of ϕ by frequency and polarization sweeps using wide-field illumination of an array of printed nanocrystals. Each molecule is represented by a short line, centered at its spatial coordinates and aligned parallel to its transition dipole angle ϕ. The color of the lines encodes the corresponding resonance frequency. The scale bar shows 4 μm. *ii-iv*: Close-ups for three exemplary NCs. The underlying image illustrates the PDF of the lateral position of the emitter, similar to Figure 2e. The scale bars are 200 nm. (d) Distribution of the angles between transition dipole moments ϕ in one NC. Dashed line shows a fit corresponding to two possible alignments of molecules, parallel or separated by 29° (see Supporting Information). (e) Spatial distribution of 261 DBT molecules with respect to the center of their corresponding NCs. The most likely orientation of DBT is set to the horizontal axis and can be associated with the *b*-axis of Ac.

setup for this measurement. A half-wave plate (HWP) and a quarterwave plate (QWP) are used to adjust the polarization of the laser beam, whereby the angles are defined with respect to the optical table. By using the two wave plates, we were able to compensate for frequency dependence of the final polarization introduced by the optical elements along the beam path. We

https://doi.org/10.1021/acsnano.4c02003
ACS Nano XXXX, XXX, XXX−XXX

note that the effect of Ac birefringence is negligible in our measurements because of the limited thickness of the NCs.

To minimize the uncertainty in the laser polarization angle $\Delta\theta_{exc}$ caused by chromatic effects, we carefully calibrated the wave plates at three different frequencies, ensuring that $\Delta\theta_{exc} < 1°$. We conducted frequency scans in wide-field illumination for at least 10 different polarization angles. For each measurement, Lorentzian fits were used to determine the resonance frequency and fluorescence count rate of the spectra of single molecules. The count rates were then analyzed as a function of the polarization angle θ_{exc} and fitted with a $\cos^2\theta_{exc}$ function because in the low-excitation regime, the molecular fluorescence intensity is proportional to the excitation intensity along its transition dipole, i.e., $F_{det} \propto \cos^2(\phi - \theta_{exc})$. Figure 5b displays the results for one molecule. This fitting procedure allowed us to extract ϕ for each molecule. Figure 5c(*i*) presents an overview of the outcome for molecules from 60 NCs. Each molecule is represented by a short dash, centered at its location and aligned to its transition dipole orientation ϕ. The color encodes the corresponding resonance frequency of the molecules (see scale on top). Close-ups of three NCs are displayed in Figure 5c(*ii-iv*). The underlying image illustrates the PDF of the lateral position of the emitters, similar to the one shown in Figure 2c. Here, the width of each Gaussian spot is determined from repeated measurements, reflecting the localization accuracy in long recordings.[34] This accuracy is primarily constrained by small mechanical drifts in the course of several hours.

The data in Figure 5c present a clear trend in the orientation of the molecular transition dipoles. To quantify these correlations, we analyzed the data between pairs of DBT molecules located in the same NC. The histogram of differences ($\Delta\phi$) in the dipole moment orientation between molecules for about 7700 pairs is shown in Figure 5d. We find that a significant fraction of the molecules are aligned with each other, and there are no pairs that are perpendicular to each other. However, we observe a secondary plateau in Figure 5d. To model this behavior, we regarded ϕ as an independent random variable following a probability density

$$P_\Phi(\phi) = a\mathcal{N}(\phi; 0, \sigma_0) + (1 - a)/2\mathcal{N}(\phi; \pm\phi', \sigma_1)$$

Here, $\mathcal{N}(\phi; \theta_i, \sigma_i)$ represents a Gaussian distribution with mean θ_i and standard deviation σ_i. The first term indicates a population of Φ centered at 0, while the other terms define two symmetric sidebands at $\pm\phi'$ about this primary axis. Treating the remaining quantities as free fit parameters, we obtained the best estimation as

$$P_\Phi(\phi) = 0.63\mathcal{N}(\phi; 0°, 6.0°) + 0.37/2\mathcal{N}(\phi; \pm 29°, 12.5°)$$

We attribute the population at $\phi' = \pm 29°$ to a second possible orientation for the insertion of DBT within the Ac NCs. The strong correlation observed in the alignment of DBT molecules provides compelling evidence for the single crystalline nature of the printed Ac, rather than a polycrystalline or amorphous structure where a large range of orientations would be possible.

Next, we also analyzed the spatial distribution of 261 DBT molecules within 61 NCs. In each NC, we localized at least 3 molecules and determined their location and dipole orientation, as was shown in Figure 5c. We assigned the center of each NC as the average values of the x and y coordinates for the emitters. Furthermore, we aligned the most common orientation of each NC along the x axis. Figure 5e displays the overall distribution obtained by adding the individual PDFs. We find a maximum molecule−molecule distance of approximately 850 nm (see also Supporting Information). Considering that the finite PDF widths (approximately 20 nm) lead to a broadening of the distribution, we attribute 850 nm as the upper limit for the lateral size of the printed NCs. This result is in agreement with our AFM measurements on NCs that were printed with similar parameters. We verified that there was no correlation between orientation ϕ and location.

Reduction of the crystal size can be envisioned via altering the substrate surface energy,[35] manipulating the wettability of both the substrate and printing nozzle,[36] and employing smaller tip diameters. Moreover, it is very important to counter the rapid sublimation of Ac NCs, e.g., by increasing Ac vapor pressure in a controlled environment. Lowering the substrate temperature in ambient conditions is less effective, particularly above the dew point.

CONCLUSION

Solid-state quantum emitters need a high degree of order in their environment because their intrinsically narrow optical transitions can be easily perturbed by atomic, molecular, or other nanoscopic dynamics in their surroundings, leading to frequency broadening and instability.[37] This requirement is typically very difficult to satisfy when emitters are placed close to material interfaces, e.g., in thin films or in nanocrystals. In our current work, we have characterized micro- and nanocrystals produced by electrohydrodynamic dripping with the advantage that individual crystals can be printed at a desired location, e.g., on a photonic circuit.[9] Since the crystal formation takes place within a short time of 1 s during the printing process, one might be concerned with the resulting crystal quality. Our measurements show, however, that the printing process yields high-quality crystals. Here, we used the line width and frequency center of the spectra recorded from single DBT molecules embedded in anthracene nanocrystals as well as the orientation of their transition dipole moments as a measure. We found that we could reach line widths that are less than twice broader than the Fourier limit of the bulk guest−host matrix and that spectral diffusion remains within the range of about one line width over hours.

The ability to print custom-designed thin micro- and nanocrystals holds great promise for a number of applications such as coupling to open Fabry−Perot microcavities[6] or integrated photonic circuits.[38,39] Moreover, the method can be used to form larger crystalline structures of different shapes, e.g., in the form of a waveguide or ring resonator. Future developments of the printing process as well as postprocessing of the resulting crystals, e.g., through annealing, might improve the crystal quality further.

EXPERIMENTAL SECTION

Nanoprinting. To prepare the printing nozzles, borosilicate capillaries (World Precision Instruments TW100−4) are rinsed with acetone and then dried with nitrogen gas. The capillaries are pulled (Sutter Instrument P-2000) to form ∼1.5 μ m inner tip diameters. They are subsequently coated with 50 nm titanium and 100 nm gold by electron beam evaporation. Each sample is fabricated on a borosilicate glass coverslip (170 μm thick) that was extensively cleaned by ultrasonic bath cleaning in diluted hexane and then deionized water for 30 min each, followed by O_2 plasma cleaning. To deposit each nanocrystal, a DC voltage of 300 V is applied to the nozzle for 1 s. The substrate temperature is kept at 21 °C during the

https://doi.org/10.1021/acsnano.4c02003
ACS Nano XXXX, XXX, XXX−XXX

fabrication. After the printing, a drop of 3 wt % poly(vinyl alcohol) in water is casted on the sample. We note that the faster sublimation of Ac NCs requires the polymer coating to be applied immediately after fabrication when the sample is still on the printing setup.

Printing Ink. The ink is prepared by saturating 1-octanol with zone-refined Ac (30 passes; TCI chemicals) at around 2.3 mg/mL. DBT is dissolved in 1,2,4-trichlorobenzene (TCB) at 2 μM concentration, and mixed with the Ac solution at a volume ratio of 1:10 TCB:octanol. In our previous work,[9] we used TCB as the solvent for terrylene:*p*-terphenyl NCs which showed stable emission at room temperature. However, adapting the same recipe for DBT:Ac system did not show efficient integration of DBT in the Ac. The NCs printed using TCB as the solvent, exhibited a low density of DBT with unstable optical transitions.

ASSOCIATED CONTENT

Supporting Information

The Supporting Information is available free of charge at https://pubs.acs.org/doi/10.1021/acsnano.4c02003.

Discussion on the effect of spectral diffusion on line width measurements, derivation of the fit function used for the histogram of dipole orientation differences in Figure 5d, and detailed description of crystal size estimation in Figure 5e (PDF)

AUTHOR INFORMATION

Corresponding Author

Vahid Sandoghdar − *Max Planck Institute for the Science of Light, D-91058 Erlangen, Germany; Department of Physics, Friedrich Alexander University Erlangen-Nuremberg, D-91058 Erlangen, Germany;* orcid.org/0000-0003-2594-4801; Email: vahid.sandoghdar@mpl.mpg.de

Authors

Mohammad Musavinezhad − *Max Planck Institute for the Science of Light, D-91058 Erlangen, Germany; Department of Physics, Friedrich Alexander University Erlangen-Nuremberg, D-91058 Erlangen, Germany;* orcid.org/0000-0002-6208-4161

Jan Renger − *Max Planck Institute for the Science of Light, D-91058 Erlangen, Germany*

Johannes Zirkelbach − *Faculty of Physics, Ludwig-Maximilians−Universität München, D-85748 Garching, Germany*

Tobias Utikal − *Max Planck Institute for the Science of Light, D-91058 Erlangen, Germany*

Claudio U. Hail − *California Institute of Technology, Pasadena, California 91125, United States;* orcid.org/0000-0001-6553-5135

Thomas Basché − *Department of Chemistry, Johannes Gutenberg-University, 55099 Mainz, Germany*

Dimos Poulikakos − *Laboratory of Thermodynamics in Emerging Technologies, Department of Mechanical and Process Engineering, ETH Zurich, CH-8092 Zurich, Switzerland;* orcid.org/0000-0001-5733-6478

Stephan Götzinger − *Max Planck Institute for the Science of Light, D-91058 Erlangen, Germany; Department of Physics, Friedrich Alexander University Erlangen-Nuremberg, D-91058 Erlangen, Germany; Graduate School in Advanced Optical Technologies (SAOT), Friedrich Alexander University Erlangen-Nuremberg, D-91052 Erlangen, Germany;* orcid.org/0000-0003-4975-0112

Complete contact information is available at: https://pubs.acs.org/10.1021/acsnano.4c02003

Funding

Open access funded by Max Planck Society.

Notes

The authors declare no competing financial interest.

ACKNOWLEDGMENTS

This work was supported by the Max Planck Society, Deutsche Forschungsgemeinschaft (TRR 306 (QuCoLiMa)), and Bundesministerium für Bildung und Forschung (RouTe Project (13N14839)). We thank Alexey Shkarin for providing the lab control software and fruitful discussions.

REFERENCES

(1) Türschmann, P.; Le Jeannic, H.; Simonsen, S. F.; Haakh, H. R.; Götzinger, S.; Sandoghdar, V.; Lodahl, P.; Rotenberg, N. Coherent nonlinear optics of quantum emitters in nanophotonic waveguides. *Nanophotonics* **2019**, *8*, 1641−1657.

(2) Toninelli, C.; et al. Single organic molecules for photonic quantum technologies. *Nat. Mater.* **2021**, *20*, 1615−1628.

(3) Moerner, W. E.; Kador, L. Optical detection and spectroscopy of single molecules in a solid. *Phys. Rev. Lett.* **1989**, *62*, 2535−2538.

(4) Orrit, M.; Bernard, J. Single pentacene molecules detected by fluorescence excitation in a p-terphenyl crystal. *Phys. Rev. Lett.* **1990**, *65*, 2716−2719.

(5) Chu, X.-L.; Götzinger, S.; Sandoghdar, V. A single molecule as a high-fidelity photon gun for producing intensity-squeezed light. *Nat. Photonics* **2017**, *11*, 58−62.

(6) Pscherer, A.; Meierhofer, M.; Wang, D.; Kelkar, H.; Martín-Cano, D.; Utikal, T.; Götzinger, S.; Sandoghdar, V. Single-Molecule Vacuum Rabi Splitting: Four-Wave Mixing and Optical Switching at the Single-Photon Level. *Phys. Rev. Lett.* **2021**, *127*, 133603.

(7) Haakh, H. R.; Faez, S.; Sandoghdar, V. Polaritonic normal-mode splitting and light localization in a one-dimensional nanoguide. *Phys. Rev. A* **2016**, *94*, 053840.

(8) Awschalom, D.; et al. Development of Quantum Interconnects (QuICs) for Next-Generation Information Technologies. *PRX Quantum* **2021**, *2*, 017002.

(9) Hail, C. U.; Höller, C.; Matsuzaki, K.; Rohner, P.; Renger, J.; Sandoghdar, V.; Poulikakos, D.; Eghlidi, H. Nanoprinting organic molecules at the quantum level. *Nat. Commun.* **2019**, *10*, 1880.

(10) Fleury, L.; Gruber, A.; Dräbenstedt, A.; Wrachtrup, J.; von Borczyskowski, C. Low-Temperature Confocal Microscopy on Individual Molecules near a Surface. *J. Phys. Chem. B* **1997**, *101*, 7933−7938.

(11) Smit, R.; Tebyani, A.; Hameury, J.; van der Molen, S. J.; Orrit, M. Sharp zero-phonon lines of single organic molecules on a hexagonal boron-nitride surface. *Nat. Commun.* **2023**, *14*, 7960.

(12) Wolters, J.; Sadzak, N.; Schell, A. W.; Schröder, T.; Benson, O. Measurement of the Ultrafast Spectral Diffusion of the Optical Transition of Nitrogen Vacancy Centers in Nano-Size Diamond Using Correlation Interferometry. *Phys. Rev. Lett.* **2013**, *110*, 027401.

(13) Galliker, P.; Schneider, J.; Eghlidi, H.; Kress, S.; Sandoghdar, V.; Poulikakos, D. Direct printing of nanostructures by electrostatic autofocussing of ink nanodroplets. *Nat. Commun.* **2012**, *3*, 890.

(14) Schneider, J.; Rohner, P.; Galliker, P.; Raja, S. N.; Pan, Y.; Tiwari, M. K.; Poulikakos, D. Site-specific deposition of single gold nanoparticles by individual growth in electrohydrodynamically-printed attoliter droplet reactors. *Nanoscale* **2015**, *7*, 9510−9519.

(15) Kress, S. J. P.; Antolinez, F. V.; Richner, P.; Jayanti, S. V.; Kim, D. K.; Prins, F.; Riedinger, A.; Fischer, M. P. C.; Meyer, S.; McPeak, K. M.; Poulikakos, D.; Norris, D. J. Wedge Waveguides and Resonators for Quantum Plasmonics. *Nano Lett.* **2015**, *15*, 6267−6275.

(16) Guymon, G. G.; Sharp, D.; Cohen, T. A.; Gibbs, S. L.; Manna, A.; Tzanetopoulos, E.; Gamelin, D. R.; Majumdar, A.; MacKenzie, J.

D. Electrohydrodynamic Printing-Based Heterointegration of Quantum Dots on Suspended Nanophotonic Cavities. *Adv. Mater. Technol.* **2024**, *9*, 2301921.
(17) Musavinezhad, M.; Shkarin, A.; Rattenbacher, D.; Renger, J.; Utikal, T.; Götzinger, S.; Sandoghdar, V. Quantum Efficiency of Single Dibenzoterrylene Molecules in p-Dichlorobenzene at Cryogenic Temperatures. *J. Phys. Chem. B* **2023**, *127*, 5353−5359.
(18) Nicolet, A. A. L.; Hofmann, C.; Kol'chenko, M. A.; Kozankiewicz, B.; Orrit, M. Single Dibenzoterrylene Molecules in an Anthracene Crystal: Spectroscopy and Photophysics. *ChemPhysChem* **2007**, *8*, 1215−1220.
(19) Taylor, R. W.; Sandoghdar, V. Interferometric Scattering Microscopy: Seeing Single Nanoparticles and Molecules via Rayleigh Scattering. *Nano Lett.* **2019**, *19*, 4827−4835.
(20) Chung, H.-R.; Kwon, E.; Oikawa, H.; Kasai, H.; Nakanishi, H. Effect of solvent on organic nanocrystal growth using the reprecipitation method. *J. Cryst. Growth* **2006**, *294*, 459−463.
(21) Shkarin, A. AlexShkarin/pyLabLib, *Zenodo*, 2023. DOI: 10.5281/zenodo.8418353.
(22) Pazzagli, S.; Lombardi, P.; Martella, D.; Colautti, M.; Tiribilli, B.; Cataliotti, F. S.; Toninelli, C. Self-Assembled Nanocrystals of Polycyclic Aromatic Hydrocarbons Show Photostable Single-Photon Emission. *ACS Nano* **2018**, *12*, 4295−4303.
(23) Gmeiner, B.; Maser, A.; Utikal, T.; Götzinger, S.; Sandoghdar, V. Spectroscopy and microscopy of single molecules in nanoscopic channels: spectral behavior vs. confinement depth. *Phys. Chem. Chem. Phys.* **2016**, *18*, 19588−19594.
(24) Basché, T.; Moerner, W.; Orrit, M. *Single-Molecule Optical Detection, Imaging and Spectroscopy*; John Wiley & Sons, 2008.
(25) Weisenburger, S.; Sandoghdar, V. Light microscopy: an ongoing contemporary revolution. *Contemp. Phys.* **2015**, *56*, 123−143.
(26) Nicolet, A. A. L.; Bordat, P.; Hofmann, C.; Kol'chenko, M. A.; Kozankiewicz, B.; Brown, R.; Orrit, M. Single Dibenzoterrylene Molecules in an Anthracene Crystal: Main Insertion Sites. *ChemPhysChem* **2007**, *8*, 1929−1936.
(27) Hettich, C.; Schmitt, C.; Zitzmann, J.; Kühn, S.; Gerhardt, I.; Sandoghdar, V. Nanometer Resolution and Coherent Optical Dipole Coupling of Two Individual Molecules. *Science* **2002**, *298*, 385−389.
(28) Trebbia, J.-B.; Deplano, Q.; Tamarat, P.; Lounis, B. Tailoring the superradiant and subradiant nature of two coherently coupled quantum emitters. *Nat. Commun.* **2022**, *13*, 2962.
(29) Lange, C. M.; Daggett, E.; Walther, V.; Huang, L.; Hood, J. D. Superradiant and subradiant states in lifetime-limited organic molecules through laser-induced tuning. *Nat. Phys.* **2024**, *20*, 836.
(30) Maser, A.; Gmeiner, B.; Utikal, T.; Götzinger, S.; Sandoghdar, V. Few-photon coherent nonlinear optics with a single molecule. *Nat. Photonics* **2016**, *10*, 450−453.
(31) Tian, Y.; Navarro, P.; Orrit, M. Single Molecule as a Local Acoustic Detector for Mechanical Oscillators. *Phys. Rev. Lett.* **2014**, *113*, 135505.
(32) Shkarin, A.; Rattenbacher, D.; Renger, J.; Hönl, S.; Utikal, T.; Seidler, P.; Götzinger, S.; Sandoghdar, V. Nanoscopic Charge Fluctuations in a Gallium Phosphide Waveguide Measured by Single Molecules. *Phys. Rev. Lett.* **2021**, *126*, 133602.
(33) Esteso, V.; Duquennoy, R.; Ng, R.; Colautti, M.; Lombardi, P.; Arregui, G.; Chavez-Angel, E.; Sotomayor-Torres, C.; Garcia, P.; Hilke, M.; Toninelli, C. Quantum Thermometry with Single Molecules in Nanoprobes. *PRX Quantum* **2023**, *4*, 040314.
(34) Deschout, H.; Zanacchi, F. C.; Mlodzianoski, M.; Diaspro, A.; Bewersdorf, J.; Hess, S. T.; Braeckmans, K. Precisely and accurately localizing single emitters in fluorescence microscopy. *Nat. Methods* **2014**, *11*, 253−266.
(35) Markov, I. V. *Crystal Growth for Beginners: Fundamentals of Nucleation, Crystal Growth and Epitaxy*; World Scientific, 2016.
(36) Wu, L.; Dong, Z.; Li, F.; Zhou, H.; Song, Y. Emerging Progress of Inkjet Technology in Printing Optical Materials. *Adv. Opt. Mater.* **2016**, *4*, 1915−1932.
(37) Schofield, R. C.; Burdekin, P.; Fasoulakis, A.; Devanz, L.; Bogusz, D. P.; Hoggarth, R. A.; Major, K. D.; Clark, A. S. Narrow and Stable Single Photon Emission from Dibenzoterrylene in para-Terphenyl Nanocrystals. *ChemPhysChem* **2022**, *23*, No. e202100809.
(38) Rattenbacher, D.; Shkarin, A.; Renger, J.; Utikal, T.; Götzinger, S.; Sandoghdar, V. On-chip interference of scattering from two individual molecules. *Optica* **2023**, *10*, 1595−1601.
(39) Ren, P.; Wei, S.; Liu, W.; Lin, S.; Tian, Z.; Huang, T.; Tang, J.; Shi, Y.; Chen, X.-W. Photonic-circuited resonance fluorescence of single molecules with an ultrastable lifetime-limited transition. *Nat. Commun.* **2022**, *13*, 3982.

https://doi.org/10.1021/acsnano.4c02003
ACS Nano XXXX, XXX, XXX−XXX